Available online at www.sciencedirect.com
SCIENCE DIRECT
International Journal of Multiphase Flow 32 (2006) 1–19
International Journal of Multiphase Flow
www.elsevier.com/locate/ijmulflow

Heat transfer to air–water annular flow in a horizontal pipe

R. Zimmerman, M. Gurevich, A. Mosyak, R. Rozenblit, G. Hetsroni *

Department of Mechanical Engineering, Technion-Israel Institute of Technology, Haifa 32000, Israel

Received 3 March 2005; received in revised form 12 September 2005

Abstract

Two-phase air–water flow and heat transfer in a 25 mm internal diameter horizontal pipe were investigated experimentally. The water superficial velocity varied from 24.2 m/s to 41.5 m/s and the air superficial velocity varied from 0.02 m/s to 0.09 m/s. The aim of the study was to determine the heat transfer coefficient and its connection to flow pattern and liquid film thickness. The flow patterns were visualized using a high speed video camera, and the film thickness was measured by the conductive tomography technique. The heat transfer coefficient was calculated from the temperature measurements using the infrared thermography method. It was found that the heat transfer coefficient at the bottom of the pipe is up to three times higher than that at the top, and becomes more uniform around the pipe for higher air flow-rates. Correlations on local and average Nusselt number were obtained and compared to results reported in the literature. The behavior of local heat transfer coefficient was analyzed and the role of film thickness and flow pattern was clarified.

Keywords: Horizontal pipe; Heat transfer; Air-water flow pattern; Annular flow; Infrared technique

1. Introduction

Horizontal annular two-phase flow in pipes is encountered in a number of industrial processes. Common applications include chemical plants, evaporators, oil wells and pipelines, fluidized bed combustors (FBC), evaporators and so on. A state of the art application is the direct steam generation (DSG) process, where steam is obtained in parabolic troughs exposed to solar energy. Sun rays are concentrated in a water circulating pipe by a parabolic reflector. In the region of high heat flux, the heating may cause high pipe wall temperatures that can damage the coating of the pipe, affecting the overall efficiency of the process. A water film around the pipe wall, as obtained in annular flow, is essential to increase the local heat transfer coefficient.

When air and water flow simultaneously in a horizontal circular pipe, different flow regimes can be distinguished. A mechanistic model for predicting flow regime transitions in two-phase gas liquid horizontal flow was presented by Taitel and Dukler (1976). They presented a flow regime map based on physical concepts and compared it to that presented by Mandhane et al. (1974) based on experimental data. Two-phase flow

* Corresponding author. Tel.: +972 48 292058; fax: +972 48 238101.
E-mail address: hetsroni@technix.technion.ac.il (G. Hetsroni).

0301-9322/$ - see front matter
doi:10.1016/j.ijmultiphaseflow.2005.09.001

pattern was also studied by Barnea and Taitel (1986), Hewitt and Ishii (1982) and Lin and Hanratty (1987). Taitel (1990) presented a unified flow pattern model that is valid for the whole range of pipe inclination angle. The annular flow regime is characterized by a gas core flowing along the center of the pipe, and a wavy liquid film that "climbs" and wets the pipe wall. In contrast to the vertical case, where the film thickness is uniform around the pipe, in the horizontal case the film is thicker on the bottom as a result of gravity. Part of the liquid flows as drops entrained in the gas core. The annular flow may be closed or open. In the closed case the film wets the entire pipe perimeter, while in the open case dryout appears at the upper part of the pipe. The present study is focused on closed or almost closed annular flow regimes.

Heat transfer and pressure drop are strongly dependent on the water film thickness and void fractions. Interfacial measurements in stratified types of flow were carried out by Ursenbacher et al. (2004). The non-intrusive computerized image analysis and optical observation method was applied to a round horizontal tube for measuring cross-sectional dry angles and void fractions. This technique yields void fractions with a measured precision in absolute value on the order of ± 0.01 over the range from 0.05 to 0.95. Dry angles were accurate to about $\pm 10°$. A significant effort has been made in the last decades to measure and calculate water film thickness and to study the structure of the gas–liquid interface by experimental and analytical/numerical methods. Badie et al. (2000) measured the film thickness and liquid film holdup in a 78 mm diameter tube using a gamma densitometer system. Luninski et al. (1983) determined the film thickness in a 8.15 mm diameter pipe by measuring the resistance of the film. They compared the results with a new model proposed, and calculated theoretically the liquid film holdup. Fukano and Ousaka (1989) performed the measurements in a 26 mm diameter pipe, using the needle contact method. In a later work, Fukano et al. (1997) studied the annular flow regime and measured the time dependent film thickness in a 19.2 mm diameter pipe by using the constant current method. They investigated the effect of the disturbance waves on the annular flow regime. Jayanti et al. (1990) analyzed the time dependent variations of liquid film thickness in a tube of 32 mm diameter using a conductance probes. They made frequency analysis of the liquid film and analyzed different mechanisms of annular pattern formation. The structure of the liquid film was investigated by Hewitt et al. (1990) using the refractive index matching technique. They used a fluorinated ethylene propylene tube of 32 mm internal diameter and squared on the external side. This material has almost the same refractive index as water so that the water film can be visualized with little distortion of the light. They found that the water film contained large number of air bubbles of all sizes, which extend right up to the wall. Bubbles were continuously entrained and released from the liquid film, enhancing the heat and mass transfer between the two phases. Shedd (2001) measured the water film thickness in a 25.4 mm diameter horizontal pipe, in the same velocity range as in the present work. The measurements were done using an optical technique. Due to the nature of the measurements, the results exclude the large waves and air–water clusters, so that the thickness reported reflect only the thin base film that exists between the large liquid waves. Therefore, the film thickness measured is thinner compared to the averaged film thickness measured in the present work, which includes the effect of the waves on film thickness.

One of the most important design parameters involved in the different applications of two-phase flow pipes is the heat transfer coefficient. Most of the literature abounds with studies of two-phase flow hydrodynamics and flow boiling, while limited data are available on the circumferential heat transfer coefficient variation in a horizontal tube. Styrikovich and Miropolski (1950) were the first to document a study of circumferential temperature variations around a horizontal tube. They found the temperature difference between the pipe top and bottom to vary with the superficial liquid and gas velocities. In the region of intermittent flow regime, Johnson and Abou-Sabe (1952) measured the average heat transfer coefficient using thermocouples. They found its dependence on air and water flow-rate. The circumferential temperature profile was measured at several axial locations by Rounthwaite (1968) in a 41.3 mm diameter pipe uniformly heated. In his work, the local heat transfer coefficient at the pipe top and bottom was reported.

Bar-Cohen et al. (1983) presented a critical review of the preceding data available for the circumferential temperature variation in horizontal boiler tubes. They concluded that minimization of the pipe top-to-bottom temperature difference is associated with the onset of annular flow regime in the tube. In a later study, Bar-Cohen et al. (1987) measured the wall temperature along a 6 m long 25.4 mm diameter pipe proving their earlier conclusions. A numerical two dimensional CFD model of a vertical wavy film induced by an upward gas flow was solved by Jayanti and Hewitt (1997). The model is valid for a vertical annular flow due to the fact

that the film thickness is very small compared to the pipe radius. They found that the heat transfer coefficient in the wave region is higher due to higher turbulence, concluding that disturbance waves are packets of turbulence transported along the tube by the gas phase that enhance the heat transfer mechanism. Although in the present study the flow is horizontal, disturbance waves exist in the flow and they contribute to cool the pipe wall as well. In more recent studies, the heat transfer coefficients for boiling (Kattan et al., 1998) were correlated. The correlations in the two cases were based on flow pattern and are valid for different flow regimes including the annular flow. They were compared to databases with ten refrigerants, obtaining a deviation of up to 20%. The infrared thermography technique was used by Mosyak and Hetsroni (1999), Hetsroni et al. (1998a,b), to investigate dryout and heat transfer in horizontal and inclined tubes in the intermittent flow regime.

The present research continues the studies carried out by Hetsroni et al. (2001, 2003) where the flow regimes and heat transfer in air–water flow in a 8° inclined tube of 25 mm diameter were investigated. In their work, a correlation for the local heat transfer coefficient was found. The same experimental facility was used here for the horizontal pipe case. A comparison between the results obtained in the inclined tube, to those measured in the present research for the horizontal tube, is presented in the study.

It is interesting to note that no previous uniform circumferential temperature measurements were found in the horizontal annular flow regime. In fact, the temperatures in all the previous published researches were averaged or measured in 2 or 3 points (top, bottom and side) around the pipe perimeter. No previous measurements of heat transfer coefficient were found in the literature for the flow of superficial velocities range that the present study deals with. The aim of this study is to measure the heat transfer coefficient and to understand its relation to the film thickness and flow pattern. The understanding of the hydrodynamics and the heat transfer mechanism of the flow is essential to improve the design of various applications.

2. Experimental facility and measurement techniques

A schematic diagram of the experimental facility is presented in Fig. 1. The water was drawn from a water tank (1) by a centrifugal pump (2). The water flow-rate was controlled by a flow regulator (3) and measured by a calibrated rotameter (4) with an accuracy of ±2%. The air was delivered by a compressor (5) through a reservoir (6) and a filter (7). The air flow-rate was regulated by a valve (8) and measured by an air velocity transducer (9). The transducer is basically an anemometer that measured the air velocity at the center of the pipe with an accuracy of ±2%. The water and the air were mixed in a mixing chamber (10) and the two-phase mixture passed through the 25 mm i.d. pipeline of the flow development section (11). Then the flow entered the flow visualization section (12) where hydrodynamic patterns were recorded by means of a high speed video camera (19) through the glass wall of the pipe. The video images were analyzed by detecting the edges of flow disturbance in a sequence of video frames. In each run a sequence of at least 120 s was recorded at a recording rate of 250 fps. In the playback mode, typical flow patterns were frozen on a TV monitor and analyzed frame by frame. The film thickness was measured using the conductive tomography instrumentation (13). Afterwards, the flow entered the heated section (14) where the wall temperature was measured using an infrared camera (18). Finally, an outlet section (15) led the water to an accumulation tank (17). The bulk temperature of the flow was measured by a mercury-in-glass thermometer (16). The air was released from the tank to the atmosphere. The whole pipe length is 8.2 m from the mixing chamber (10) to the accumulation tank (17), including the 4 m long development section (11), the 1.8 m long outlet section (15) (that were made of plastic tubes), the section for flow visualization and the heated test section (1.2 m long each).

The film thickness was measured using the conductive tomography technique developed at the University of Hannover, Germany (Hetsroni et al., 2003) with an accuracy of 0.01 mm. With this technique the conductivity of the liquid film between two electrodes, is measured. The voltage is calibrated to the liquid film thickness. Since for film thickness less than 0.01 mm the calibration could not be performed properly, it is assumed that in the region of 0–0.01 mm the voltage varied linearly with the film thickness. The electrodes are installed flush with the inner pipe surface at six different positions around the pipe circumference. Single-phase airflow test were conducted by Hetsroni et al. (2003), using the same facility with an 8° pipe inclination to establish the validity of the system and the test technique.

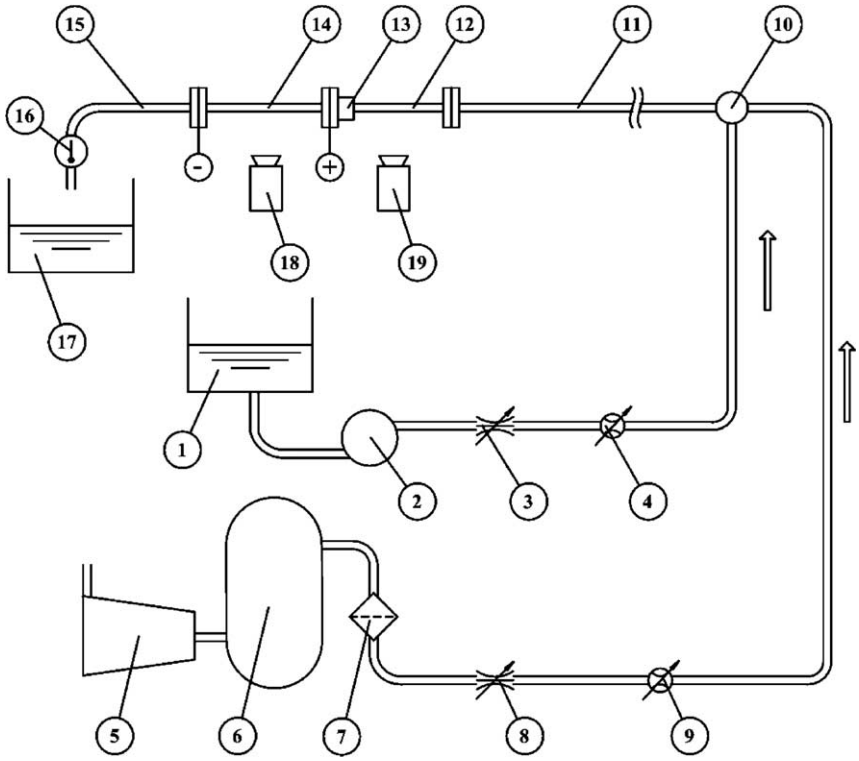

Fig. 1. Experimental facility: (1) water tank; (2) centrifugal pump; (3) water flow regulator; (4) rotameter; (5) compressor; (6) reservoir; (7) air filter; (8) air regulator; (9) air velocity transducer; (10) mixing chamber; (11) flow development section; (12) flow visualization section; (13) conductive tomography instrumentation; (14) heated section; (15) outlet section; (16) thermometer; (17) accumulation tank; (18) infrared camera; (19) high speed video camera.

A thermal imaging radiometer was used to remotely measure the pipe wall temperature by detecting infrared radiation from the heated surface in the wavelength range of 8–12 μm. The detector of the radiometer is cooled by an integrated cooler to 77 K for maximum thermal sensitivity and high spatial resolution. A sufficient amount of energy is radiated from the pipe to allow a calibration of this instrument in order to make highly accurate, non-contact, temperature measurements. The heater was coated with paint which is black in the infrared range. Through calibration, the thermal imaging radiometer is very accurate, obtaining a measured temperature with an accuracy of ±1 K. The air–water mixture bulk temperature was measured with an accuracy of ±0.5 K.

Special attention was paid to the design of the heated section in order to obtain a negligible heat transfer in the axial and circumferential directions that can distort the heat transfer coefficient calculation. Therefore, it was constructed from a 50 μm thick stainless steel foil. The heated section had a length of 1.2 m and it is shown in Fig. 2. Preliminary calculations (Hetsroni and Rozenblit, 1994) have shown that the difference between the temperature of the two sides of the thin foil (inside wall temperature and outside wall temperature), was less than 0.1 K. In this manner the inside wall surface temperature could be known by measuring the outside wall surface temperature. Hetsroni et al. (2001, 2003) calculated the axial heat conduction for the heated test section using measurements of wall temperature distribution in the streamwise direction. The heat transfer in the axial direction was less than 0.5% of that in the radial one. They also estimated the total heat losses that were in the range of 3–4%, depending on the values of the heat flux. A DC current obtained from a controlled power supply was applied to the foil to obtain the desired heat flux. The test conditions are given in Table 1. Fig. 3 shows flow regime map reported by Lin and Hanratty (1987) for air and water flowing in horizontal pipe of inner diameter 2.54 cm and experimental conditions of the present study.

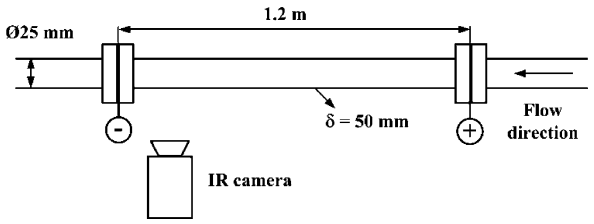

Fig. 2. Heated pipe section.

Table 1
Experimental conditions

U_L (m/s)	U_G (m/s)	T_0 (°C)	q (W/m^2)
0.020	36.3	19.8	6260
0.020	41.5	19.6	8600
0.028	24.2	21.4	5800
0.028	36.3	20.9	11300
0.028	41.5	20.4	11100
0.045	24.2	22.7	11800
0.045	36.3	22.2	11900
0.045	41.5	21.6	11600
0.090	24.2	23.8	19500
0.090	36.3	24.0	23200
0.090	41.5	24.1	22600

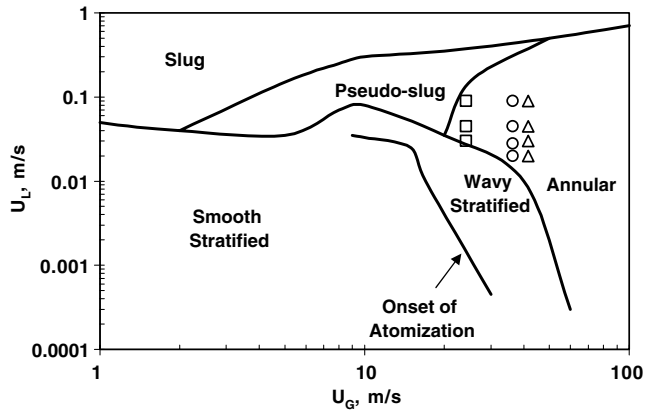

Fig. 3. Flow regime map.

3. Results

A number of verification runs were undertaken prior to the data logging. A series of tests for single-phase air and water flow were conducted to establish the validity of the system and test technique. The experimental results agreed well with those calculated by Kays (1966) for fully developed turbulent flow in a tube. Effect of wall thickness on heat transfer coefficient was studied also by Mosyak et al. (2001). It was shown that the wall temperature fluctuations were influenced by the thermal properties and thickness of the wall but the average wall temperature and heat transfer coefficient were independent of the wall thickness. The measurements in two-phase flow were performed for different air–water flow regimes. The water superficial velocity changed in the range from 0.020 m/s to 0.090 m/s while the air superficial velocity varied from 24.2 m/s to 41.5 m/s.

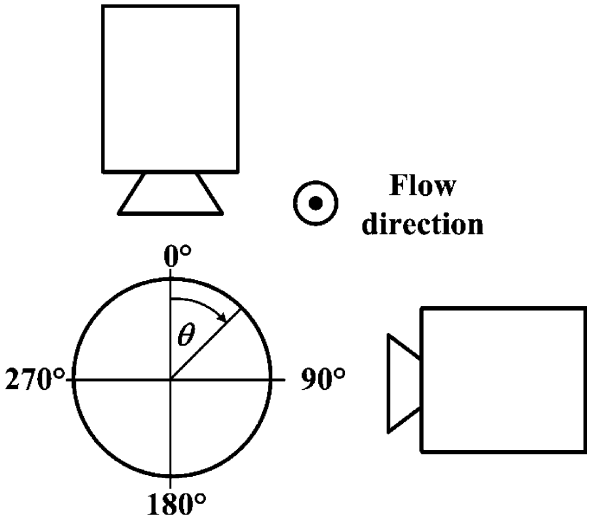

Fig. 4. Angle of the measurements and camera orientations.

Most flow regimes in the pipe were closed or almost closed annular flow for all cases studied. Fig. 4 shows the camera angular orientations, and the definition of the angle of the measurements θ.

3.1. Analytical considerations

In order to understand the flow behavior and its influence on the heat transfer phenomenon, attention was focused on the physical parameters that are relevant to the problem. The physical variables involved in the equations of motion and energy that affect the flow pattern and the heat transfer are: the liquid and gas superficial velocities (U_L and U_G), the pipe diameter (D), the liquid and gas densities and viscosities (ρ_L, ρ_G, μ_L and μ_G), the acceleration due to gravity (g), the liquid surface tension (σ), the pipe roughness (ε), the liquid and gas thermal conductivities (k_L and k_G), the liquid and gas specific heats (c_{pL} and c_{pG}), the flow bulk temperature (T_0), the pipe wall heat flux (q'') and the local heat transfer coefficient (α). Applying the Buckingham Pi-theorem to the equations of momentum and energy, the independent dimensionless groups that govern the physical behavior of the flow and the heat transfer were found. From all the independent groups, the more relevant were chosen to present the experimental data. The choice was based on a physical analysis of the phenomenon and on a reasonable guess of the parameters used to describe the experimental data by a common curve. The non-dimensional parameters chosen for the analysis are

$$Re_G = \frac{U_G D \rho_G}{\mu_G}; \qquad Fr_L = \frac{U_L^2}{gD}; \qquad Nu_L = \frac{\alpha D}{k_L} \tag{1}$$

where Re_G is the gas based Reynolds number, Fr_L the liquid based Froude number and Nu_L the liquid based Nusselt number.

In theoretical researches into the circumferential distribution of the liquid film thickness in gas–liquid horizontal two-phase flow, the discussion has been focused on the mechanisms for transferring liquid towards the top of the tube. A detailed mechanism that liquid is transferred in the circumferential direction has not been proposed so far, though it is understood that the disturbance waves play the most important role. It is difficult to connect the liquid film thickness to heat transfer because the annular flow is highly unsteady in the disturbance wave region. In keeping with the Taitel and Dukler (1976) model, a detailed analysis performed by Weisman et al. (1979) revealed that the major influences on the flow patterns in horizontal pipes are the liquid and gas superficial velocities, liquid properties and pipe diameter.

The experiments were performed maintaining a difference between the wall temperature in the heated section and the flow mean temperature below 20 °C. The temperatures of the heated tube wall and of the fluid

varied in the range from 20 °C to 40 °C. From here, it is assumed that surface tension, density, viscosity, and thermal conductivity of the fluids, remained constant during the experiments. This fact implies that the flow pattern and the heat transfer coefficient were not affected by the heat flux or by the dependence of thermal properties of the fluids on the temperature. The heat transfer and flow parameters for each data run were measured under steady-state conditions, and as a result of the temperature range the heat was transferred to the flow without phase change.

For engineering purposes, the macroscopic behavior of the flow and the heat transfer are more meaningful than the microscopic details. Therefore, Eulerian averaging was applied to eliminate information concerning the local instantaneous fluctuation of the data. The film thickness and temperature measurements were repeated five times for each case, and then the value was averaged using

$$f = \frac{1}{\tau}\int_0^{\tau} f(\tau)\,\mathrm{d}\tau \approx \frac{1}{n}\sum_{i=1}^{n} f(\tau_i) \tag{2}$$

where f is the measured variable, τ is the time and n is the number of measurements.

For the time and space mean value, within the angle range from 0 to π, the calculation was done using

$$f = \frac{1}{\tau\pi}\int_0^{\pi}\int_0^{\tau} f(\theta,\tau)\,\mathrm{d}\tau\,\mathrm{d}\theta \approx \frac{1}{n\pi}\int_0^{\pi}\sum_{i=1}^{n} f(\tau_i)\,\mathrm{d}\theta \tag{3}$$

3.2. Flow pattern

The annular flow consists of a water film around the pipe and an air core. It is important to note that the film appears as a wavy pattern that slowly moves along the wall. The height of a wave may reach some times the undisturbed liquid film. When a wave becomes big enough, interface forces aid air to mix with water, forming an aerated mass of liquid called air–water cluster, as can be seen in Fig. 5(a). Clusters move along the pipe with the flow, faster than the liquid film and slower than the gas core. They are separated from one another by the thinner and slower wavy liquid film. Some of the disturbance waves, that constitute the wavy pattern of the film, appear sometimes equidistant as it can be seen in Fig. 5(b) where three little waves are seen in the picture. But not always a periodic pattern appeared, and single waves were seen between the air–water clusters. It can be concluded that within the annular pattern, the flow presents a disordered configuration. Some of the waves seen, disappeared as they were swallowed by faster waves or as a consequence of disturbance wave amplitude growth. In this manner, waves join together and grow to form a cluster by mixing with the air flow. Some waves instead, disappear under surface tension and gravity effects. The clusters may reach the top of the pipe, forming a full pipe air–water cluster. They constitute an important contribution to the water flow, due to their size that is significant with respect to the water film thickness. Therefore, they cannot be ignored, as drop entrainment into the gas core cannot be ignored when accounting for the liquid flow-rate.

In the case of smaller superficial velocities, droplets appeared at the top of the pipe as can be seen in Fig. 5(a). It is the open annular flow regime with motionless or slowly moving droplets. Spedding et al. (1998) referred this regime to ''film plus droplet pattern''. For those cases, lift forces are not strong enough to bring the water film to the top of the pipe to form a closed annular flow pattern. In some cases droplets attached to the pipe wall in the top dryout area were distinguished (see Fig. 5(a)). These droplets are brought to the upper wall by entrainment to the air flow and deposition to the wall afterwards. They travel slower than the liquid film due to surface tension and adhesion forces that maintain them attached to the pipe wall. Their contribution to the heat transfer mechanism is very significant.

3.3. Film thickness

Applying the conductive tomography method, the water film thickness δ was measured as a function of the pipe angle. The data was measured from $\theta = 0°$ to 360° in increments of 60°. The results are shown in Fig. 6(a)–(d), where the film thickness is plotted as a function of the pipe angle, for all the regimes tested. The results of half of the pipe are plotted (from $\theta = 0°$ to 180°) since the measurements were symmetrically

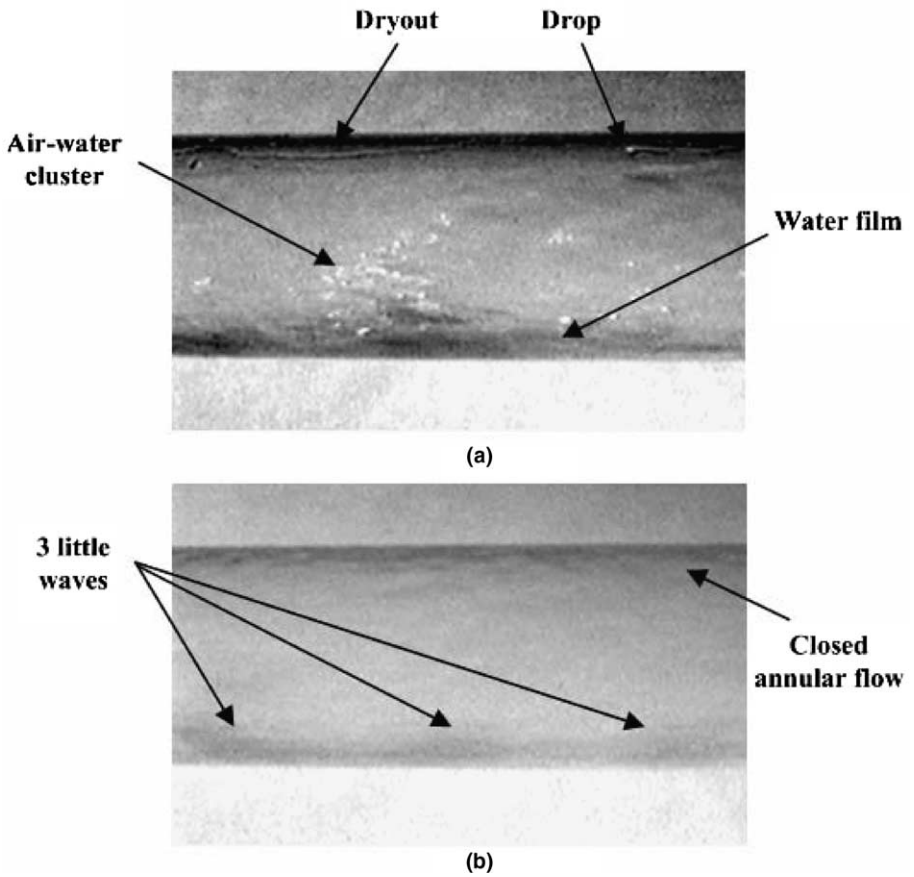

Fig. 5. Flow regime: $U_G = 36.3$ m/s. (a) $U_L = 0.020$ m/s and (b) $U_L = 0.090$ m/s.

distributed about the middle of the pipe as expected. The film thickness data measured is summarized in Table 2.

The wavy pattern of the film, including waves and air–water clusters, causes a time dependent film thickness. In this work the analysis is done for a time averaged film thickness. In all cases the film is thicker at the bottom, decreasing with the circumferential angle, due to gravity. The film thickness at the bottom of the pipe gets significantly thinner with air superficial velocity growth as seen in Fig. 6(a)–(d). In contrast, at the top of the pipe, the film thickness increases with air flow-rate until it reaches a certain value (around 400 μm). The film thickness does not change anymore for further increase of the air superficial velocity in the range of the superficial velocities used in the present work. It seems that a physical limit of film thickness is approached. This limit is a result of gravitational forces. When film thickness is increased beyond a critical value, the gravitational forces overcome lifting forces, impeding the water to "climb" the pipe wall and helping the entrainment/deposition mechanism to cause water to re-enter the gas core as droplets. Therefore, gravity acts as a limiting force that impedes film growth at the top of the pipe beyond a certain thickness. The uniformity in the film thickness around the pipe is due more to the thinning of the film at the bottom than to circumferential redistribution. It can be concluded that the film thickness becomes more uniform around the pipe with air flow-rate increase as concluded by Fukano and Ousaka (1989) and Jayanti et al. (1990).

By contrast, the higher the water flow-rate is, the thicker the water film becomes at the bottom of the pipe. For a higher liquid superficial velocity, air flow must be greater in order to cause a uniform film thickness around the pipe, because a higher lift force and a larger entrainment are required. It is remarkable that for the higher air superficial velocity, the liquid film thickness at the top of the pipe is almost not influenced by the liquid superficial velocity. The reason of this behavior is gravity.

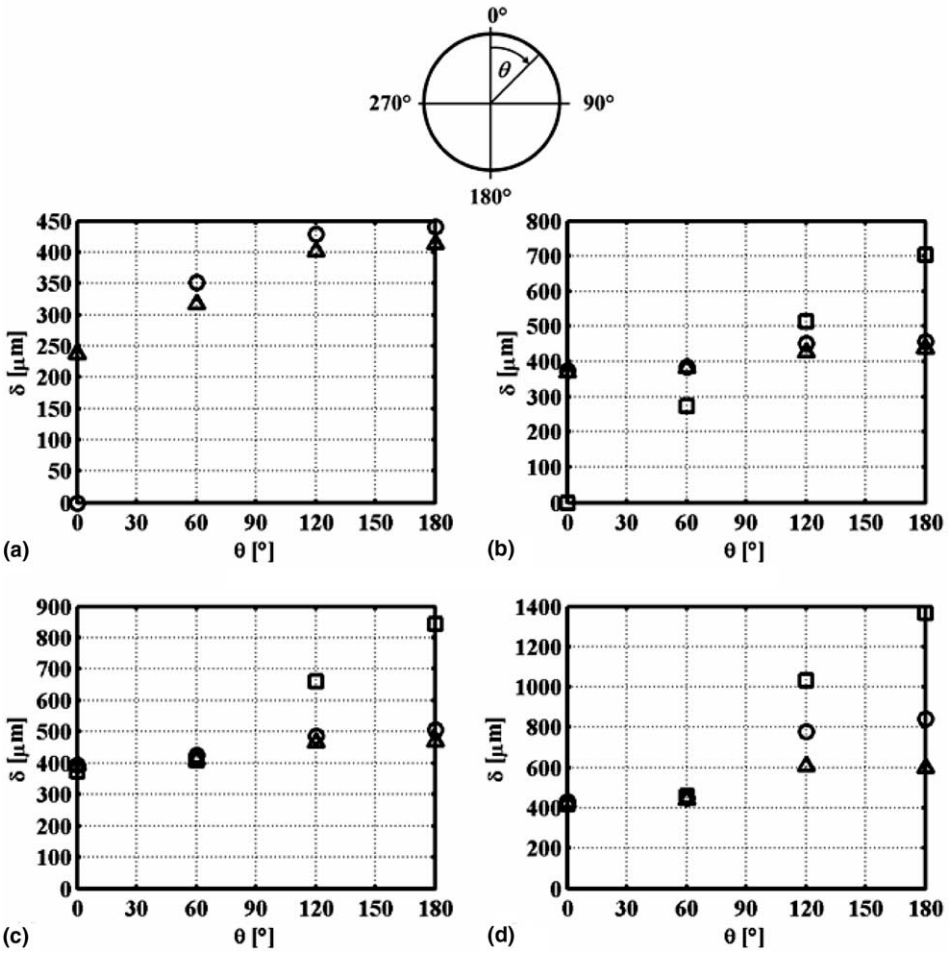

Fig. 6. Time averaged water film thickness: (□) $U_G = 24.2$ m/s; (○) $U_G = 36.3$ m/s; (△) $U_G = 41.5$ m/s. (a) $U_L = 0.020$ m/s, (b) $U_L = 0.028$ m/s, (c) $U_L = 0.045$ m/s and (d) $U_L = 0.090$ m/s.

Table 2
Liquid film thickness δ (μm)

U_L (m/s)	U_G (m/s)	0°	60°	120°	180°
0.017	36.3	0	352	429	440
0.017	41.5	237	317	401	413
0.025	24.2	0	272	514	704
0.025	36.3	373	384	452	458
0.025	41.5	369	383	427	435
0.044	24.2	374	408	660	843
0.044	36.3	394	425	487	506
0.044	41.5	392	410	465	469
0.088	24.2	418	459	1030	1366
0.088	36.3	430	450	779	841
0.088	41.5	425	440	607	598

In the present study the term "liquid film thickness" is used as the average thickness of liquid distributed during a period t, over the over the angle θ. For given value of the angle, during this period the thickness changes due to waviness of the film, entrainment of the bubbles, etc. These changes depend on superficial

velocities of air and water and may be characterized by the relation $S = \mathrm{rms}(\delta_{av})/\delta_{av}$, where δ_{av} and δ_{av}, is the instantaneous and average value of film thickness, respectively. Fig. 7 shows the dependence of the relative film thickness S on Re_G/Re_L for different values of superficial liquid velocity. Increase in the ratio Re_G/Re_L leads to decrease of the relative film thickness S.

3.4. Liquid film holdup

For all regimes studied, the liquid film holdup was calculated as the cross-sectional area of the liquid film divided by the cross-section of the pipe (as defined by Luninski et al., 1983)

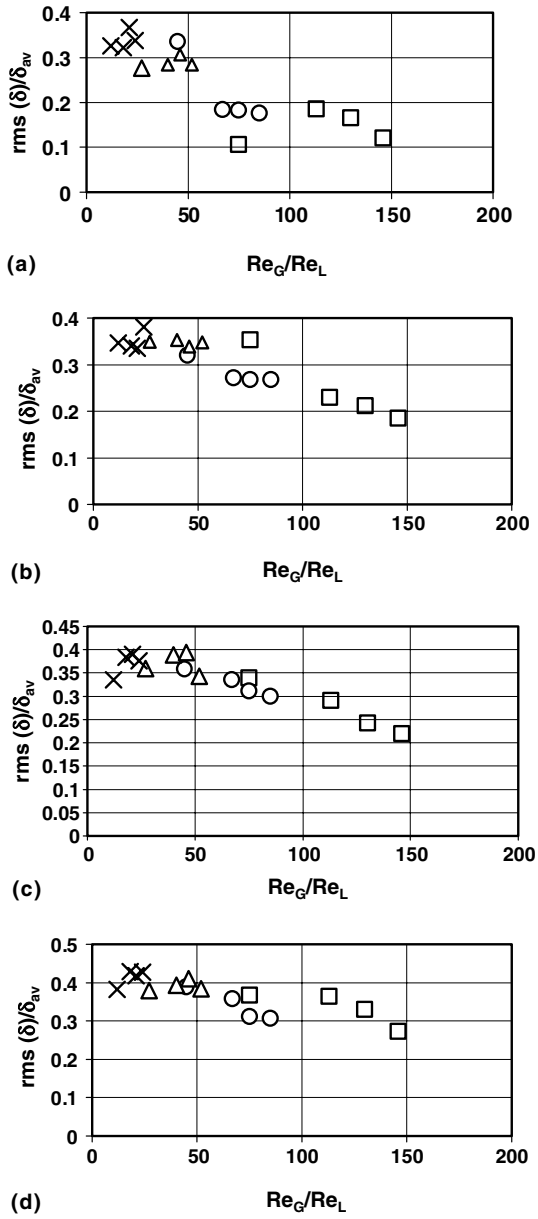

Fig. 7. Dependence of relative film thickness on Re_G/Re_L: (□) $U_L = 0.020$ m/s; (○) $U_L = 0.028$ m/s; (△) $U_L = 0.045$ m/s; (×) $U_L = 0.090$ m/s.

$$\phi = \frac{A_\delta}{A_D} = \frac{\int_0^{2\pi} \delta(\theta) \frac{D}{2} \mathrm{d}\theta}{\pi} D^2/4 \tag{4}$$

where ϕ is the liquid film holdup, A_δ the liquid film cross-sectional area and A_D the pipe cross-section. The integral was solved numerically, for six points measured around the pipe. The results obtained are plotted in Fig. 8 as a function of air superficial velocity and agree qualitatively with those presented by Luninski et al. (1983). In their study the tendency of decrease in the liquid film holdup with increasing gas flow-rate was observed for a different pipe diameter at small liquid superficial velocities. This trend is due to the fact

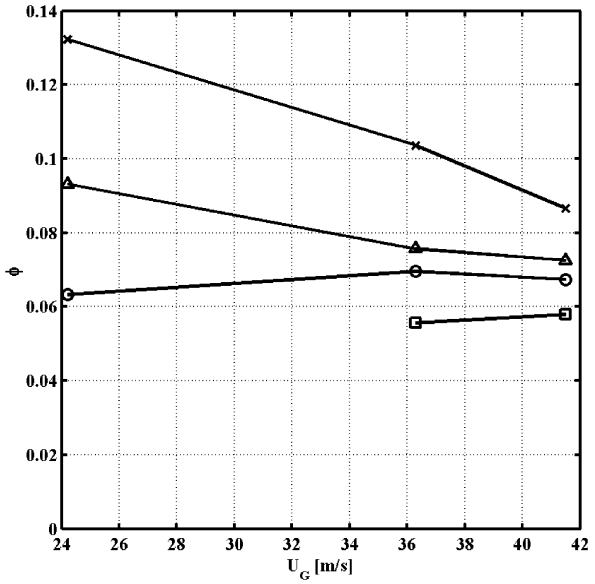

Fig. 8. Liquid film holdup vs. air superficial velocity: (□) $U_L = 0.020$ m/s; (○) $U_L = 0.028$ m/s; (△) $U_L = 0.045$ m/s; (×) $U_L = 0.090$ m/s.

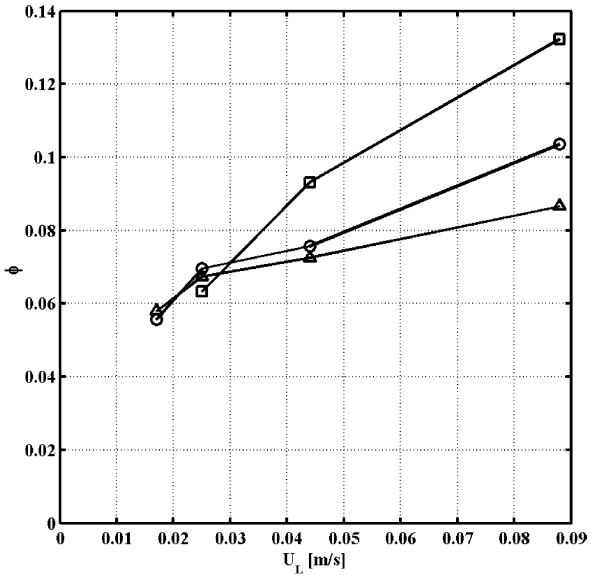

Fig. 9. Liquid film holdup vs. water superficial velocity: (□) $U_G = 24.2$ m/s; (○) $U_G = 36.3$ m/s; (△) $U_G = 41.5$ m/s.

that the higher the gas flow-rate is, the more the liquid droplets are entrained into the gas core and the stronger the waviness of the flow interface becomes, causing the appearance of higher waves and air–water clusters. These factors result in a reduction of the water flow-rate through the film.

Fig. 9 presents the liquid film holdup as a function of water superficial velocity. The same increasing growth trend of the liquid film holdup with increasing liquid flow-rate measured by Badie et al. (2000) for a different pipe diameter and smaller air superficial velocity, was obtained in the present study.

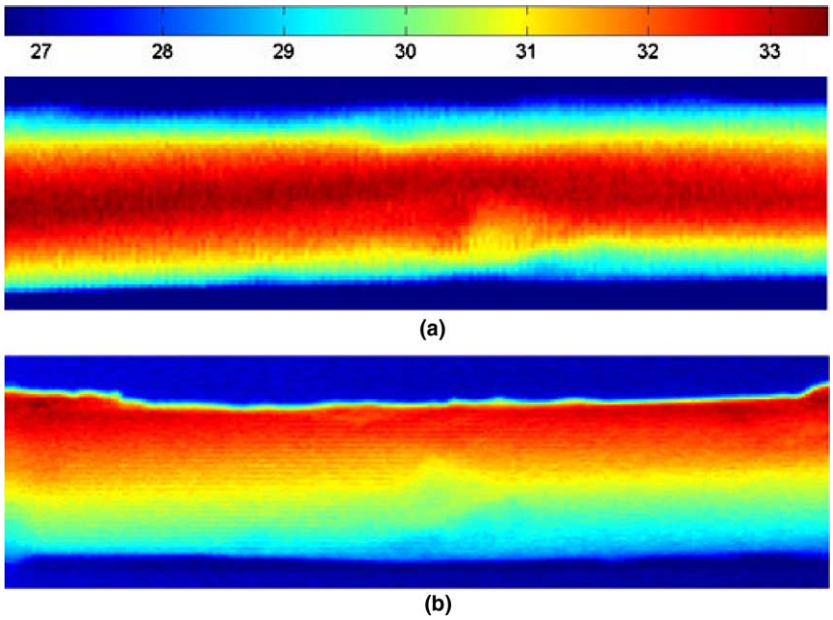

Fig. 10. Infrared image: $U_L = 0.020$ m/s; $U_G = 36.3$ m/s. (a) Top view ($\theta = 0°$) and (b) side view ($\theta = 90°$).

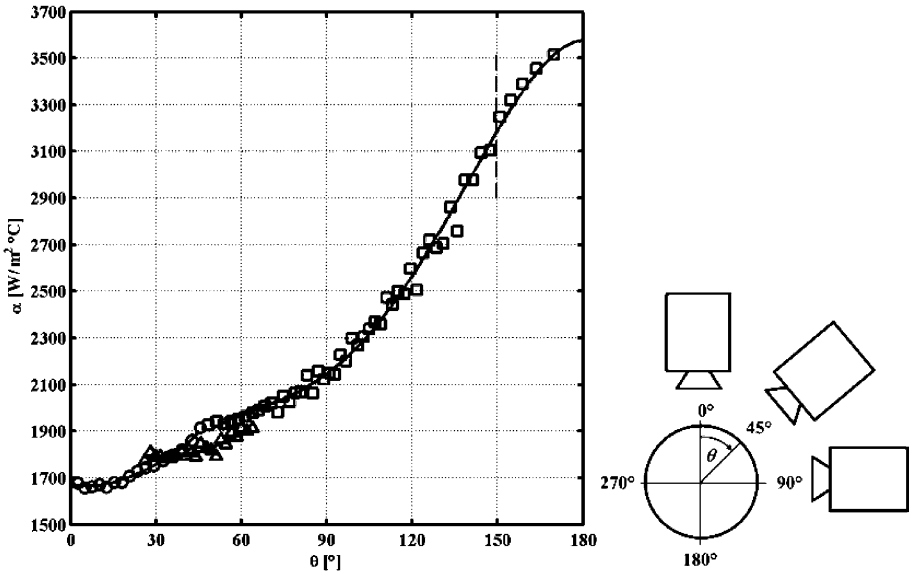

Fig. 11. Local heat transfer coefficient: $U_L = 0.090$ m/s; $U_G = 41.5$ m/s. Top, side and 45° views. (○) $\theta = 0°$; (△) $\theta = 45°$; (□) $\theta = 90°$.

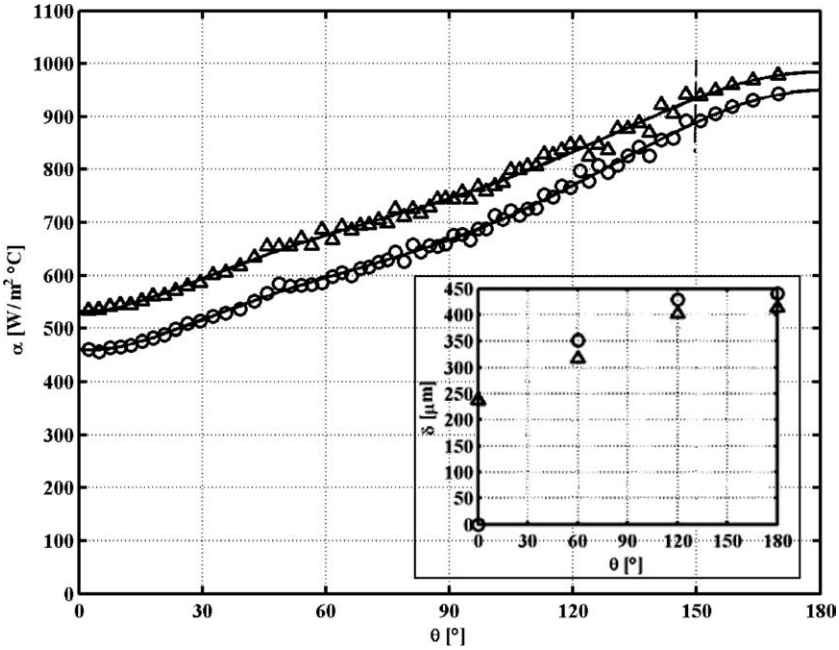

Fig. 12. Local heat transfer coefficient: $U_L = 0.020$ m/s. (○) $U_G = 36.3$ m/s; (△) $U_G = 41.5$ m/s.

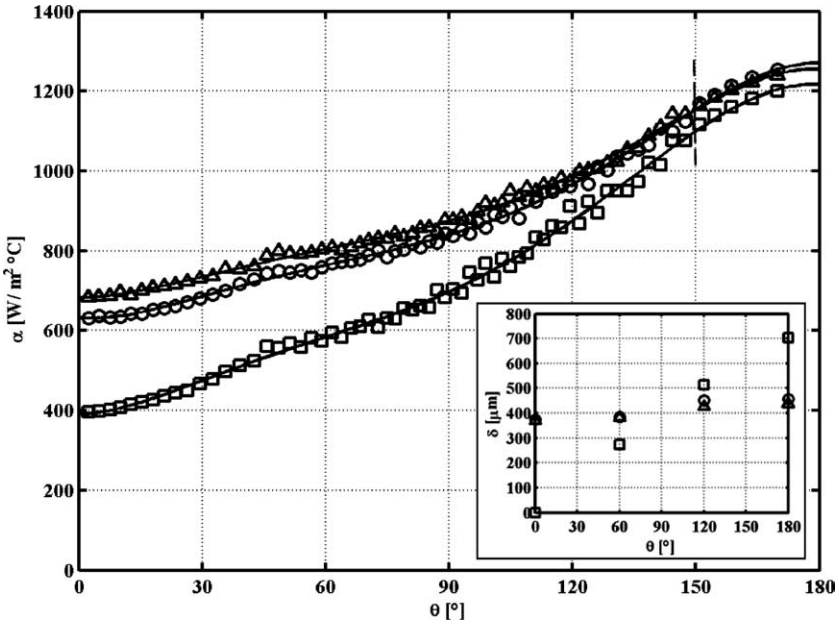

Fig. 13. Local heat transfer coefficient: $U_L = 0.028$ m/s. (□) $U_G = 24.2$ m/s; (○) $U_G = 36.3$ m/s; (△) $U_G = 41.5$ m/s.

3.5. Temperature on the heated wall

The temperature of the wall was measured using the infrared thermography method. Infrared images were taken at the end of the 1.2 m long heated pipe section were the temperature profile is fully developed. The experiments were repeated to confirm their reproducibility. For each combination of air and water superficial

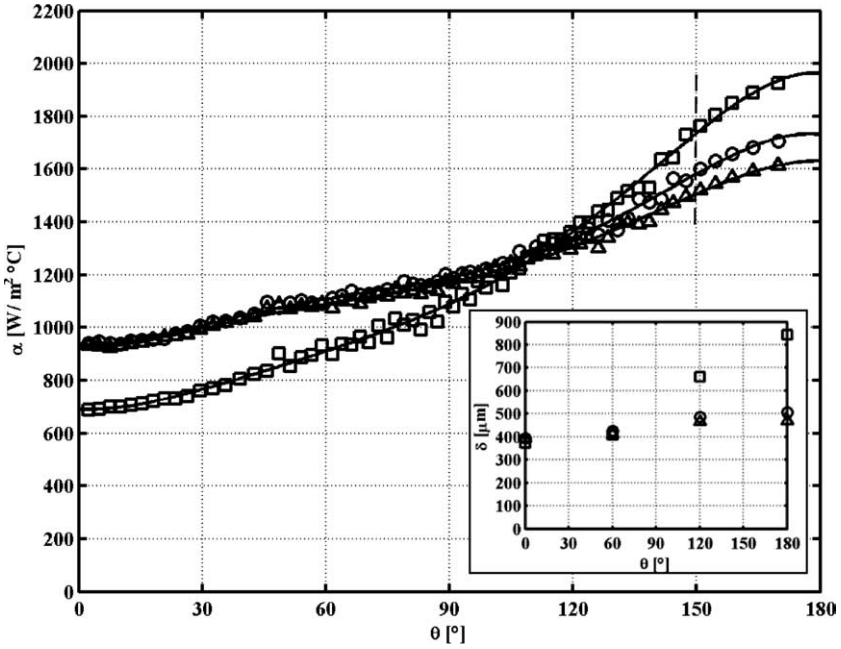

Fig. 14. Local heat transfer coefficient: $U_L = 0.045$ m/s. (□) $U_G = 24.2$ m/s; (○) $U_G = 36.3$ m/s; (△) $U_G = 41.5$ m/s.

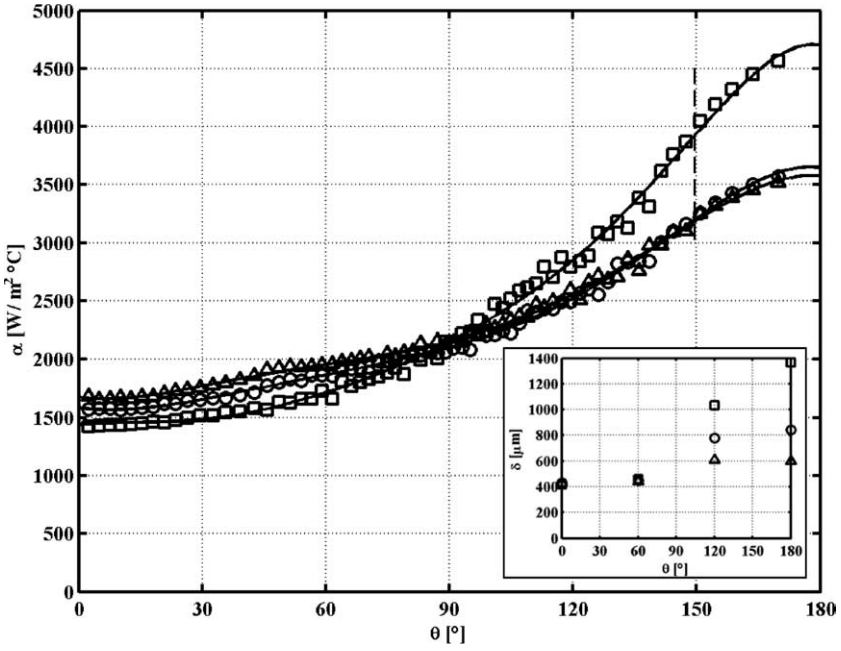

Fig. 15. Local heat transfer coefficient: $U_L = 0.090$ m/s. (□) $U_G = 24.2$ m/s; (○) $U_G = 36.3$ m/s; (△) $U_G = 41.5$ m/s.

velocities, time averaged infrared images were taken from two orientation angles: one from the top ($\theta = 0°$) and the other from the side ($\theta = 90°$) as shown in Fig. 10(a) and (b).

Although earlier studies of heat transfer in annular flow were performed under conditions close to circumferential isothermality (Styrikovich and Miropolski, 1950; Bar-Cohen et al., 1983, 1987), the results obtained in the present study showed a temperature variation from the top to the bottom of the pipe. This variation was

also measured by Hetsroni et al. (2001, 2003) for annular flow in an 8° inclined pipe. It is caused by the film thickness changing around the pipe perimeter, the waviness difference between the upper and the bottom parts of the pipe and the bubbles entrainment to the water film that depends on the waviness of the film.

3.6. Heat transfer coefficient

The local heat transfer coefficient was calculated as

$$\alpha = \frac{q''}{\overline{T_W} - \overline{T_0}} \tag{5}$$

where α is the heat transfer coefficient, q'' is the pipe wall heat flux, $\overline{T}_W$ is the time averaged pipe wall temperature at a given angle, and $\overline{T}_0$ the time averaged bulk flow temperature. The bulk flow temperature was determined as following: the gas temperature and gas humidity was measured at the inlet and outlet of the experimental setup. According these measurements the average bulk flow temperature and the change of enthalpy was determined. The heat transfer coefficients were calculated with an accuracy of 15%. No infrared images of the pipe were taken from the bottom orientation ($\theta = 180°$), hence the heat transfer coefficient was extrapolated by a second order polynomial with the same slope of the preceding curve at $\theta = 150°$, and with a null slope at $\theta = 180°$ due to symmetry of the temperature profile. The boundary of this region is indicated by dashed line.

Infrared images were taken from a camera orientation of $\theta = 45°$ for one of the flow-rates ($U_L = 0.090$ m/s and $U_G = 41.5$ m/s). Fig. 11 shows the local heat transfer coefficient calculated in this case, from the three different camera orientation measurements. It is seen that the error in the heat transfer calculation caused by the view factor at this angle is about 5%, and therefore the images were taken only from two orientations ($\theta = 0°$ and 90°) for all the cases. It should be taken into account that the little "hump" that appears for $\theta = 45°$ in all the heat transfer plots, is caused by this error and it has no additional physical meaning.

The local heat transfer coefficients are shown in Figs. 12–15 for different air and water superficial velocities. The experimental data are presented in Table 3. The circumferential distribution of the local heat transfer coefficient on the pipe wall varies significantly in each flow regime. The heat transfer coefficient increases from the top of the pipe ($\theta = 0°$) to the bottom ($\theta = 180°$), being up to three times higher at the lower part. A similar

Table 3
Heat transfer coefficient α (W/m^2 K)

U_L (m/s)	0.02	0.02	0.028	0.028	0.028	0.045	0.045	0.045	0.09	0.09	0.09
U_G (m/s)	36.3	41.5	24.2	36.3	41.5	24.2	36.3	41.5	24.2	36.3	41.5
θ (°)	$\alpha \times 10^{-3}$ (W/m^2 K)										
0	0.46	0.53	0.39	0.63	0.68	0.69	0.94	0.93	1.44	1.59	1.68
10	0.47	0.54	0.41	0.64	0.69	0.7	0.94	0.93	1.46	1.57	1.67
20	0.49	0.56	0.44	0.66	0.71	0.73	0.97	0.96	1.46	1.6	1.71
30	0.52	0.59	0.48	0.69	0.74	0.77	1.01	1	1.49	1.66	1.77
40	0.55	0.62	0.51	0.71	0.76	0.81	1.05	1.03	1.54	1.73	1.84
50	0.57	0.65	0.55	0.74	0.78	0.86	1.08	1.06	1.61	1.8	1.9
60	0.6	0.68	0.58	0.76	0.8	0.91	1.11	1.09	1.72	1.87	1.96
70	0.62	0.7	0.62	0.79	0.83	0.96	1.14	1.12	1.84	1.94	2.02
80	0.64	0.72	0.66	0.81	0.85	1.02	1.16	1.14	1.99	2.02	2.08
90	0.67	0.75	0.7	0.84	0.88	1.09	1.19	1.17	2.15	2.1	2.16
100	0.7	0.77	0.75	0.87	0.91	1.17	1.23	1.21	2.35	2.21	2.26
110	0.73	0.8	0.81	0.92	0.94	1.26	1.28	1.25	2.58	2.35	2.39
120	0.77	0.83	0.88	0.97	0.99	1.36	1.34	1.31	2.85	2.52	2.56
130	0.81	0.87	0.95	1.03	1.04	1.48	1.41	1.37	3.18	2.73	2.75
140	0.85	0.9	1.03	1.09	1.1	1.61	1.5	1.44	3.55	2.96	2.97
150	0.89	0.93	1.1	1.15	1.15	1.74	1.58	1.51	3.94	3.21	3.19
160	0.92	0.96	1.16	1.21	1.21	1.85	1.66	1.57	4.32	3.44	3.39
170	0.94	0.98	1.2	1.26	1.24	1.94	1.72	1.62	4.61	3.61	3.54
180	0.95	0.98	1.22	1.27	1.26	1.96	1.73	1.63	4.7	3.65	3.58

tendency was measured by Hetsroni et al. (2001, 2003) for a 8° upward inclined pipe. This irregularity is due to the distribution of the air and water phases in the pipe. The gravity forces caused the liquid film to be thicker at the bottom of the pipe. Another factor that caused such a behavior of the local heat transfer was the waviness and the entrainment of bubbles to the water film. Both phenomena are more significant at the lower part of the tube. When air was entrained to the liquid film, as was shown by Hewitt et al. (1990), the turbulence of the film increased and the bubbles caused a decrease in the local thickness of the viscous boundary layer, contributing to the local heat transfer coefficient enhancement. Our results showed that the heat transfer was enhanced when liquid or air superficial velocity increased.

The measurements of liquid film thickness revealed that the film thickness in the upper part of the pipe was almost not affected by the air superficial velocity when the thickness reached about 400 μm. Therefore the changes in the heat transfer coefficient there were mainly due to the waviness of the film. In the lower tube part, besides the waves influence, the bubbles entrained to the film also increase the heat transfer mechanism. The thickness of the film also caused a heat transfer enhancement because the thicker the film was, the higher the waves became, causing a rise in the turbulence of the flow and a stronger air entrainment to the film.

Despite the fact that under certain flow conditions a complete liquid annulus was not formed and dryout areas at the top of the pipe appeared (Fig. 5(a)), droplets or liquid streaks wetted the pipe wall there. Furthermore very small droplets entrained in the gas phase increased its effective heat capacity. As a result the heat transfer coefficient did not drop dramatically at the dryout location.

In Fig. 16(a)–(d) the local heat transfer coefficients are compared to those obtained in the 8° upward inclined pipe and presented by Hetsroni et al. (2001, 2003) for a gas superficial velocity $U_G = 36.3$ m/s. Their experiment was performed using the same experimental facility employed in the present research and for

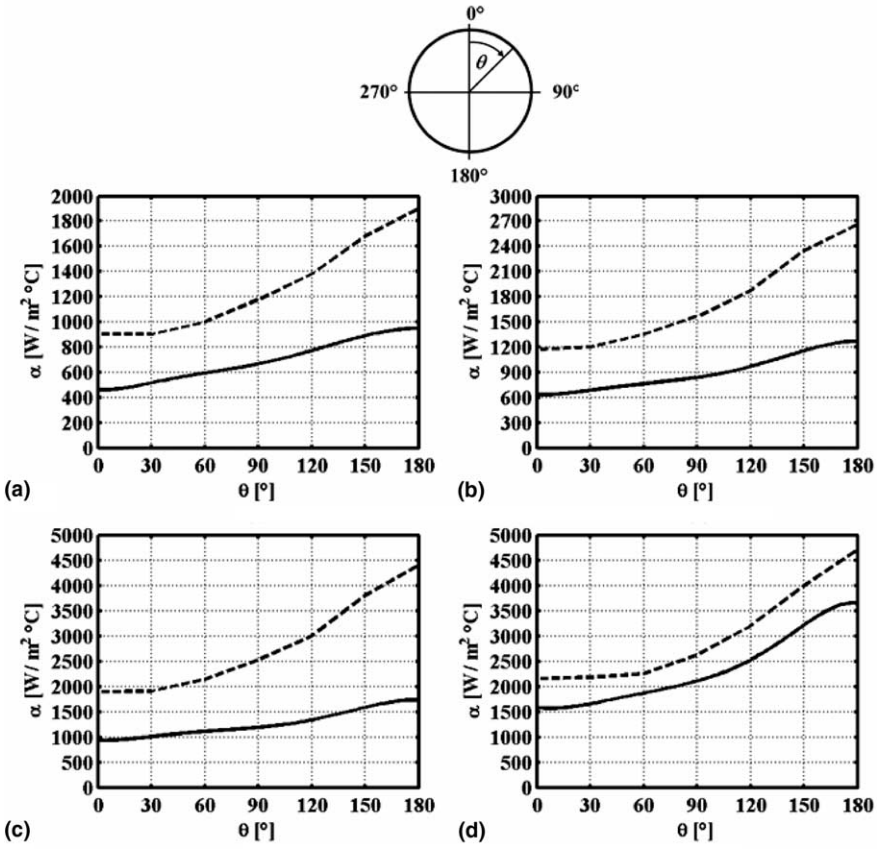

Fig. 16. Local heat transfer comparison to 8° upward inclination pipe: $U_G = 36.3$ m/s. (—) Horizontal; (---) 8° upwards. (a) $U_L = 0.020$ m/s, (b) $U_L = 0.028$ m/s, (c) $U_L = 0.045$ m/s and (d) $U_L = 0.090$ m/s.

nearly the same flow superficial velocities. The results show a clear improvement of the heat transfer coefficient with the pipe inclination. Taitel and Dukler (1976) showed that the flow regimes are very sensitive to the pipe inclination angle. In the flow regime maps presented in their work, the transition from stratified to annular flow in the inclined tube occurs for a smaller air superficial velocity than for the case of horizontal tube. The stabilizing effect of the gravity acting perpendicular to the flow diminishes when the pipe is inclined. Furthermore, a parallel to the tube axis component of the gravity vector promotes the waves formation. It is interesting to note that Styrikovich and Miropolski (1956) suggested that upward inclination of the pipe of 9.5° leads to equalization of the circumferential temperatures of the heated pipe wall. The same effect was reported by Mosyak and Hetsroni (1999). They studied the thermal and hydrodynamic phenomena in horizontal and inclined at 5° tubes. The higher circumferential wall temperature variation was measured for horizontal tube.

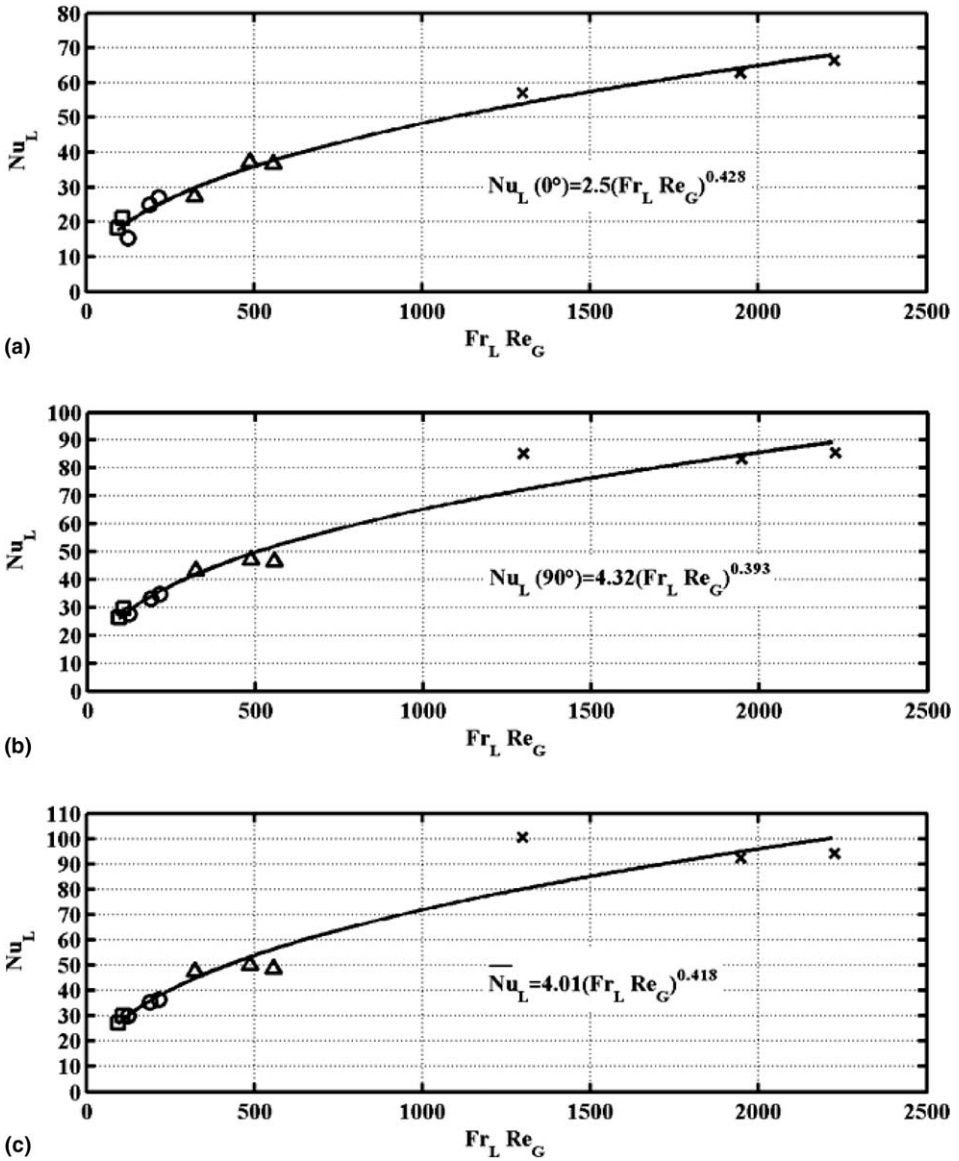

Fig. 17. Nusselt number correlation: (□) $U_L = 0.020$ m/s; (○) $U_L = 0.028$ m/s; (△) $U_L = 0.045$ m/s; (×) $U_L = 0.090$ m/s. (a) $Nu_L(\theta = 0°)$, (b) Nu_L $(\theta = 90°)$ and (c) $\overline{Nu}_L$.

Fig. 17(a) and (b) shows the dependence of the local Nusselt number, $Nu_L(0°)$ and $Nu_L(90°)$ on the parameter $Fr_L Re_G$ at $\theta = 0°$ and $\theta = 90°$, respectively. Fig. 17(c) shows dependence of the space averaged Nusselt number around the tube ($\overline{Nu}_L$) on $Fr_L Re_G$. The following equations were found to describe the experimental data:

$$Nu_L(0°) = 2.5(Fr_L Re_G)^{0.428} \tag{6}$$

$$Nu_L(90°) = 4.32(Fr_L Re_G)^{0.393} \tag{7}$$

$$\overline{Nu}_L = 4.01(Fr_L Re_G)^{0.418} \tag{8}$$

The air–water heat transfer discussed above is not strictly valid for boiling flow of water, heated by some external heat source. However, under saturation conditions, and for modest axial changes in the steam quality, the results of heat transfer in air–water flow can be expected to offer a first guide to thermal behavior of boiling flow. This assertion was discussed by Bar-Cohen et al. (1983).

4. Conclusions

A study of the flow pattern and heat transfer to air–water annular flow in a horizontal pipe of 25 mm i.d. was conducted. The water superficial velocity varied from 24.2 m/s to 41.5 m/s and the air superficial velocity varied from 0.02 m/s to 0.09 m/s.

The flow patterns were visualized by using a high speed video camera, and the film thickness was measured by the conductive tomography technique. Disturbance waves, air–water clusters and entrained droplets are part of the flow pattern structure, and were visible in the pictures. These structures, together with the bubbles entrained in the liquid film, are the main factors that influence the heat transfer from the wall to the flow.

The local heat transfer coefficient was calculated from the temperature measurements which were conducted by using infrared thermography method. The circumferential distribution of the heat transfer coefficients on the pipe wall varies significantly in the flow regimes studied. The heat transfer coefficient at the bottom of the pipe is up to three times higher than that at the top, and becomes more uniform around the pipe for higher air flow-rates.

The relationship between the local heat transfer behavior and the hydrodynamics of the flow was clarified. The liquid superficial velocity was found to be a major factor which affects the local heat transfer coefficient around the tube. The heat transfer coefficient measurements for the horizontal case were compared to the case were the pipe is slightly inclined upwards. The results show a clear improvement of the heat transfer coefficient with the pipe inclination.

Empirical correlations on local and average Nusselt number were developed. The results of the present study can be used to predict the pipe wall temperature for the heat transfer to air–water flow in a horizontal tube, in the range of superficial velocities studied here.

Acknowledgements

This research was supported by the Fund for the Promotion of Research at the Technion. A. Mosyak and R. Rozenblit are supported by a joint grant from the Center for Absorption in Science of the Ministry of Immigrant Absorption and the Committee for Planning and Budgeting of the Council for Higher Education under the framework of the KAMEA program.

References

Badie, S., Hale, C.P., Lawrence, C.J., Hewitt, G.F., 2000. Pressure gradient and holdup in horizontal two-phase gas–liquid flows with low liquid loading. Int. J. Multiphase Flow 26, 1525–1543.

Bar-Cohen, A., Ruder, Z., Griffith, P., 1983. Circumferential wall temperature variations in horizontal boiler tubes. Int. J. Multiphase Flow 9, 1–12.

Bar-Cohen, A., Ruder, Z., Griffith, P., 1987. Thermal and hydrodynamic phenomena in a horizontal, uniformly heated steam-generating pipe. J. Heat Transfer 109, 739–745.

Barnea, D., Taitel, Y., 1986. Encyclopedia of Fluid Mechanics (Cheremisinoff N.P.) Gas–Liquid Flows, vol. 3. Gulf Publishing, pp. 403–474 (Chapter 16, Flow pattern transition in two-phase gas–liquid flows).

Fukano, T., Ousaka, A., 1989. Prediction of the circumferential distribution of film thickness in horizontal and near-horizontal gas–liquid annular flows. Int. J. Multiphase Flow 15, 403–419.

Fukano, T., Nakagawa, H., Mori, Y., Watanabe, M., 1997. Liquid film formation on the inner surface of the horizontal channel. Nucl. Eng. Des. 175, 3–13.

Hetsroni, G., Rozenblit, R., 1994. Heat transfer to a liquid–solid mixture in a flume. Int. J. Multiphase Flow 20, 671–689.

Hetsroni, G., Hu, B.G., Yi, J.H., Mosyak, A., Yarin, L.P., Ziskind, G., 1998a. Heat transfer in intermittent air–water flows. Part I—horizontal tube. Int. J. Multiphase Flow 24, 165–188.

Hetsroni, G., Yi, J.H., Hu, B.G., Mosyak, A., Yarin, L.P., Ziskind, G., 1998b. Heat transfer in intermittent air–water flows. Part II—upward inclined tube. Int. J. Multiphase Flow 24, 189–212.

Hetsroni, G., Gurevich, M., Mosyak, A., Rozenblit, R., 2001. Dryout in inclined gas–liquid pipe-lines. Trans IChemE 79, 376–382.

Hetsroni, G., Mewes, D., Enke, C., Gurevich, M., Mosyak, A., Rozenblit, R., 2003. Heat transfer to two-phase flow in inclined tubes. Int. J. Multiphase Flow 29, 173–194.

Hewitt, G.F., Ishii, M., 1982. Handbook of Multiphase Systems (Hetsroni G.) Liquid–gas Systems. Hemisphere Publication Co., McGraw Hill Book Co, pp. 2.1–2.128 (Chapter 2).

Hewitt, G.F., Jayanti, S., Hope, C.B., 1990. Structure of thin liquid films in gas–liquid horizontal flow. Int. J. Multiphase Flow 16, 951–957.

Jayanti, S., Hewitt, G.F., 1997. Hydrodynamics and heat transfer in wavy annular gas–liquid flow: a computational fluid dynamics study. Int. J. Heat Mass Transfer 40, 2445–2460.

Jayanti, S., Hewitt, G.F., White, S.P., 1990. Time-dependent behavior of the liquid film in horizontal annular flow. Int. J. Multiphase Flow 16, 1097–1116.

Johnson, H.A., Abou-Sabe, A.H., 1952. Heat transfer and pressure drop for turbulent flow of air–water mixtures in a horizontal pipe. Trans. ASME, 977–987.

Kattan, N., Thome, J.R., Favrat, D., 1998. Flow boiling in horizontal tubes: Part 3—development of a new heat transfer model based on flow pattern. Trans. ASME 120, 156–165.

Kays, W.M., 1966. Convective Heat and Mass Transfer. McGraw-Hill Book Company, NY.

Lin, P.Y., Hanratty, T.J., 1987. Effect of pipe diameter on flow patterns for air–water flow in horizontal pipes. Int. J. Multiphase Flow 13, 549–563.

Luninski, Y., Barnea, D., Taitel, Y., 1983. Film thickness in horizontal annular flow. Can. J. Chem. Eng. 61, 621–626.

Mandhane, J.M., Gregory, G.A., Aziz, K., 1974. A flow pattern map for gas–liquid flow in horizontal pipes. Int. J. Multiphase Flow 1, 537–553.

Mosyak, A., Hetsroni, G., 1999. Analysis of dryout in horizontal and inclined tubes. Int. J. Multiphase Flow 25, 1521–1543.

Mosyak, A., Pogrebnyak, E., Hetsroni, G., 2001. Effect of constant heat flux boundary condition on wall temperature fluctuations. ASME J. Heat Transfer 123 (2), 213–218.

Rounthwaite, C., 1968. Two-phase heat transfer in horizontal tubes. J. Inst. Fuel 41, 66–76.

Shedd, T.A., 2001. Characteristics of the liquid film in horizontal two-phase flow. Ph.D. Thesis, University of Illinois, Urbana-Champaign.

Spedding, P.L., Watterson, J.K., Raghunathan, S.R., Ferguson, M.E.G., 1998. Two-phase co-current flow in inclined pipe. Int. J. Heat Mass Transfer 41, 4205–4228.

Styrikovich, M.A., Miropolski, Z.L., 1950. Stratification in vapor-water mixture flow at high pressures in the heated horizontal tube. Dokl. Akad. Nauk. SSSR LXXI (2) (in Russian).

Styrikovich, M.A., Miropolski, Z.L., 1956. Technical Report IGRL-T/R4.

Taitel, Y., 1990. Flow pattern transition in two phase flow. In: Proceedings of the 9th International Heat Transfer Conference, Jerusalem, vol.1, pp. 237–254 .

Taitel, Y., Dukler, A.E., 1976. A model for predicting flow regime transitions in horizontal and near horizontal gas–liquid flow. AIChE J. 22, 47–55.

Ursenbacher, T., Wojitan, L., Thome, J.R., 2004. Interfacial measurements in stratified types of flow. Part I: New optical measurement technique and dry angle measurements. Int. J. Multiphase Flow 30, 107–124.

Weisman, J., Dungan, D., Gibson, J., Crawford, T., 1979. Effects of fluid properties and pipe diameter on two-phase flow patterns in horizontal lines. Int. J. Multiphase Flow 5, 437–462.